

A Robust and Efficient Visual-Inertial Initialization with Probabilistic Normal Epipolar Constraint

Changshi Mu¹, Daquan Feng^{1†}, Qi Zheng^{1†}, and Yuan Zhuang²

Abstract— Accurate and robust initialization is essential for Visual-Inertial Odometry (VIO), as poor initialization can severely degrade pose accuracy. During initialization, it is crucial to estimate parameters such as accelerometer bias, gyroscope bias, initial velocity, and gravity, etc. The IMU sensor requires precise estimation of gyroscope bias because gyroscope bias affects rotation, velocity and position. Most existing VIO initialization methods adopt Structure from Motion (SfM) to solve for gyroscope bias. However, SfM is not stable and efficient enough in fast motion or degenerate scenes. To overcome these limitations, we extended the rotation-translation-decoupling framework by adding new uncertainty parameters and optimization modules. First, we adopt a gyroscope bias optimizer that incorporates probabilistic normal epipolar constraints. Second, we fuse IMU and visual measurements to solve for velocity, gravity, and scale efficiently. Finally, we design an additional refinement module that effectively diminishes gravity and scale errors. Extensive initialization tests on the EuRoC dataset show that our method reduces the gyroscope bias and rotation estimation error by an average of 16% and 4% respectively. It also significantly reduces the gravity error, with an average reduction of 29%.

I. INTRODUCTION

Visual-Inertial Odometry (VIO) aims to estimate the camera position in various unknown environments. It operates by fusing image information from a camera and IMU measurements from an IMU sensor. The camera can estimate a visual map and reduce pose drift. The IMU sensors provide metric scale for camera motion and also offer short-term robustness. VIO shares many advantages, such as small size, low cost, and low power consumption. These properties have led to an increasing number of applications of VIO in virtual reality [1], augmented reality [2], [3], and automated robotics [4], [5], among others.

To run a VIO system effectively, a set of parameters must be accurately estimated during the initialization stage. These parameters include the scale, gravity direction, initial velocity, and the bias of accelerometers and gyroscopes. Incorrect initialization will result in poor convergence and inaccurate estimation of all other system parameters. On the other hand, fast initialization is also important. As the VIO system cannot work until the IMU is properly initialized [6].

¹Changshi Mu, Daquan Feng, and Qi Zheng are with the Guangdong Key Laboratory of Intelligent Information Processing, College of Electronics and Information Engineering, Shenzhen University, Shenzhen 518000, China {fdquan, qiz}@szu.edu.cn, 2200432055@email.szu.edu.cn

²Yuan Zhuang is with the State Key Laboratory of Information Engineering in Surveying, Mapping and Remote Sensing, Wuhan University, Wuhan 430072, China {yuan.zhuang}@whu.edu.cn

[†]Corresponding authors

Basically, previous works on VIO initialization can be classified into tightly and loosely coupled methods. Tightly coupled methods [7], [8], [9] assume that camera poses can be approximated from IMU measurements. They fuse visual observations with IMU integration and estimate initialization parameters through a closed-form solution, which can increase computational cost. Moreover, these methods often ignore gyroscope bias, which can harm accuracy. The loosely coupled methods [6], [10], [11] assume that the camera trajectory obtained by visual SfM is very accurate. First, they solve the visual SfM problem, and initialize the inertial parameters based on the derived camera pose. Therefore, the accuracy of these methods relies heavily on the performance of visual SfM. However, in case of fast camera motion or too few common feature points, visual SfM can become unstable.

Overall, both tightly coupled and loosely coupled methods fail to fully exploit the complementary information between the camera and the IMU. Specifically, tightly coupled methods do not utilize visual observations to estimate gyroscope bias, which can lead to numerical stability issues and lower accuracy. Loosely coupled methods do not use IMU measurements to enhance the stability of visual SfM, resulting in low accuracy or initialization failure in challenging motion scenarios. Inspired by the fact that image observations can be directly used to optimize the rotation between image frames [12], [13] proposed a rotation-translation-decoupled VIO initialization method. This method enhances the connection between visual observations and IMU measurements. However, this approach overlooks the quality of image feature matches. Each match is given equal weight in the final result. Even though outliers are removed from feature matches, error distributions of 2D feature correspondences vary with image content and the specific matching technique. Therefore, it is crucial to consider the uncertainty of 2D feature matches.

To overcome the limitations of SfM and improve initialization accuracy and robustness, we estimate the gyroscope bias considering the probabilistic normal epipolar constraint (PNEC). This method enhances the accuracy of gyroscope bias estimation by accounting for anisotropic and inhomogeneous uncertainties of the feature points. Based on the rotation-translation-decoupled framework [13], we first solve the rotation. Then, we solve the translation using the linear global translation constraint (LiGT) [14]. Finally, we estimate velocity, scale, and gravity by solving a least-squares problem. To further improve the accuracy of scale and gravity, we also introduce a modified scale-gravity refinement module.

II. RELATED WORK

Initialization in VIO systems is critical because it affects the systems' accuracy and robustness. Numerous initialization methods have been proposed and applied to VIO systems (e.g., [15], [16], [11], [17]) in recent years. Martinelli [7] proposed for the first time a tightly coupled closed-form solution to jointly recover parameters including initial velocity, gravity, and feature point depth. His method assumes that common feature points can be observed in all frames during the initialization process, and IMU measurements can be used to estimate camera pose. However, this method is unsuitable for inexpensive and noisy IMU sensors as it ignores gyroscope bias. Subsequently, Kaiser et al. extended this work in [8]. They iteratively solved a nonlinear least-squares problem that includes the gravity magnitude to determine the gyroscope bias. Their experiments demonstrated that gyroscope bias affects the accuracy of closed-form solutions. Nevertheless, the tightly coupled closed-form solution suffers from low accuracy and computational efficiency in estimating gyroscope bias.

With the emergence of higher precision visual odometry or SfM [18], [19], the loosely coupled method using precise camera poses to solve IMU initialization parameters has been proposed [11], [10]. Mur-Artal and Tardós [11] process the IMU and visual initialization separately. They calculate the initial estimation of scale, gravity, velocity, and IMU biases based on a set of keyframe poses processed by the monocular SLAM algorithm. Similarly, Qin and Shen [10] proposed a linear system but set the accelerometer bias to zero in visual-inertial bundle adjustment. Both methods ignore the uncertainty of sensors and the correlation between inertial parameters. To solve this problem, Campos et al. [6] proposed a maximum-a-posteriori framework to initialize IMU parameters. Zuñiga-Noël et al. [20] proposed a non-iterative analytical solution for estimating IMU parameters within a maximum-a-posteriori framework.

III. PRELIMINARIES

A. Visual-Inertial Notation

In this paper, we define the notations as follows. The body frame and image frame at time-index i are represented by \mathbf{F}_{b_i} and \mathbf{F}_{c_i} , respectively. Let $\mathbf{R}_{b_i b_j}$ and $\mathbf{p}_{b_i b_j}$ denote the rotation and translation between the IMU frame at time index i and the IMU frame at time index j . Define the gravity vector as $\mathbf{g} = (0, 0, G)^\top$, where G is the magnitude of gravity. The camera and IMU are rigidly attached, with the transformation $\mathbf{T}_{bc} = [\mathbf{R}_{bc} | \mathbf{p}_{bc}]$ between their reference systems determined from calibration. $[\cdot]_\times$ and $\|\cdot\|$ denote the skew-symmetric operation and the Euclidean norm operation.

At two time points corresponding to image frames \mathbf{F}_{b_i} and \mathbf{F}_{b_j} , we pre-integrate linear acceleration and angular velocity within the local frame \mathbf{F}_{b_i} . Let $\boldsymbol{\alpha}_{b_j}^{b_i}$, $\boldsymbol{\beta}_{b_j}^{b_i}$, $\boldsymbol{\gamma}_{b_j}^{b_i}$ represent the pre-integration of translation, velocity, and rotation from \mathbf{F}_{b_i} to \mathbf{F}_{b_j} :

$$\boldsymbol{\alpha}_{b_j}^{b_i} = \sum_{k=i}^{j-1} \left(\left(\sum_{f=i}^{k-1} \mathbf{R}_{b_i b_f} \mathbf{a}_f^m \Delta t \right) \Delta t + \frac{1}{2} \mathbf{R}_{b_i b_k} \mathbf{a}_k^m \Delta t^2 \right) \quad (1)$$

$$\boldsymbol{\beta}_{b_j}^{b_i} = \sum_{k=i}^{j-1} \mathbf{R}_{b_i b_k} \mathbf{a}_k^m \Delta t \quad (2)$$

$$\boldsymbol{\gamma}_{b_j}^{b_i} = \prod_{k=i}^{j-1} \text{Exp}(\boldsymbol{\omega}_k^m \Delta t) \quad (3)$$

where $\text{Exp}(\cdot)$ stands for the exponential map $\text{Exp} : \mathfrak{so}(3) \rightarrow SO(3)$. $\boldsymbol{\omega}_k^m$ and \mathbf{a}_k^m represent the gyroscope and accelerometer measurements at time k respectively, and Δt denotes the time interval between successive IMU data. The above pre-integration formula is independent of the bias. We use the rotation pre-integration update formula in [21]. The effect of the gyroscope bias \mathbf{b}_g on the rotation pre-integration $\boldsymbol{\gamma}_{b_j}^{b_i}$ can be expressed as a first-order Taylor approximation:

$$\hat{\boldsymbol{\gamma}}_{b_j}^{b_i} = \boldsymbol{\gamma}_{b_j}^{b_i} \text{Exp} \left(\mathbf{J}_{\mathbf{b}_g}^{\boldsymbol{\gamma}_{b_j}^{b_i}} \mathbf{b}_g \right) \quad (4)$$

where $\mathbf{J}_{\mathbf{b}_g}^{\boldsymbol{\gamma}_{b_j}^{b_i}}$ denotes the Jacobian of the derivative of $\boldsymbol{\gamma}_{b_j}^{b_i}$ with respect to \mathbf{b}_g . This Jacobian is a constant that can be efficiently computed iteratively [21]. In this work, we ignore the accelerometer bias as in [8] since this has little effect on the initialization result.

The motion between two consecutive keyframes can be computed by integrating the inertial measurements. We use the standard approach on $SO(3)$ manifold described in [21]:

$$\mathbf{p}_{c_0 b_j} = \mathbf{p}_{c_0 b_i} + \mathbf{v}_{b_i}^{c_0} \Delta t_{ij} - \frac{1}{2} \mathbf{g}^{c_0} \Delta t_{ij}^2 + \mathbf{R}_{c_0 b_i} \boldsymbol{\alpha}_{b_j}^{b_i} \quad (5)$$

$$\mathbf{v}_{b_j}^{c_0} = \mathbf{v}_{b_i}^{c_0} - \mathbf{g}^{c_0} \Delta t_{ij} + \mathbf{R}_{c_0 b_i} \boldsymbol{\beta}_{b_j}^{b_i} \quad (6)$$

$$\mathbf{R}_{c_0 b_j} = \mathbf{R}_{c_0 b_i} \boldsymbol{\gamma}_{b_j}^{b_i} \quad (7)$$

where $\mathbf{R}_{c_0 b_j}$ denotes the rotation from image frame at time-index 0 (i.e., the first image frame) to the IMU frame at time-index j . $\mathbf{p}_{c_0 b_j}$ represents the corresponding translation. $\mathbf{v}_{b_j}^{c_0}$ and \mathbf{g}^{c_0} denote the IMU velocity at time-index j and gravity in the \mathbf{F}_{c_0} coordinate system, respectively. Δt_{ij} is the time interval from time-index i to time-index j .

B. Background – NEC

In the following, we review the main idea of the normal epipolar constraint (NEC) proposed in [22]. The NEC describes the feature constraint between two image frames. This constraint is composed of the bearing vectors of the two frames and the normal vectors of the corresponding epipolar plane. As shown in Fig. 1, when two consecutive image frames \mathbf{F}_{c_i} and \mathbf{F}_{c_j} observe the same 3D point \mathbf{p}_k , \mathbf{F}_{c_i} and \mathbf{F}_{c_j} as well as the 3D point \mathbf{p}_k define an epipolar plane. The associated normal vector of this plane is $\mathbf{n}_k = [\mathbf{f}_i^k]_\times \mathbf{R}_{c_i c_j} \mathbf{f}_j^k$. \mathbf{f}_i^k and \mathbf{f}_j^k are unit bearing vectors pointing from \mathbf{F}_{c_i} and \mathbf{F}_{c_j} to \mathbf{p}_k , respectively. All normal vectors

are perpendicular to the translation vector $\mathbf{p}_{c_i c_j}$, collectively defining the epipolar normal plane. It means that, ideally, all normal vectors are coplanar. Therefore, we can establish the residual of the constraint based on the normalized epipolar error:

$$e_k = \left| \mathbf{p}_{c_i c_j}^\top \mathbf{n}_k \right| \quad (8)$$

where $\mathbf{p}_{c_i c_j}$ denotes the translation vector from \mathbf{F}_{c_i} to \mathbf{F}_{c_j} . The geometry of the residual is expressed as the Euclidean distance from the normal vector to the epipolar normal plane. The NEC energy function can be constructed with this residual:

$$E(\mathbf{R}_{c_i c_j}, \mathbf{p}_{c_i c_j}) = \sum_k e_k^2 = \sum_k \left| \mathbf{p}_{c_i c_j}^\top \left([\mathbf{f}_i^k]_\times \mathbf{R}_{c_i c_j} \mathbf{f}_j^k \right) \right|^2 \quad (9)$$

The relative rotation $\mathbf{R}_{c_i c_j}$ is estimated by ensuring the coplanarity of the normal vectors. Assuming that the two image frames jointly observe n 3D points, we can compute n normal vectors of the epipolar plane and stack them into a matrix $\mathbf{N} = [\mathbf{n}_1 \dots \mathbf{n}_n]$. The requirement for coplanarity is mathematically expressed by the condition that the minimum eigenvalue of the matrix $\mathbf{M} = \mathbf{N} \mathbf{N}^\top$ is zero. Thus, the problem of solving the rotation can be parameterized as:

$$\begin{aligned} \mathbf{R}_{c_i c_j}^* &= \underset{\mathbf{R}_{c_i c_j}}{\operatorname{argmin}} \lambda_{\mathbf{M}_{ij}, \min} \\ \text{with } \mathbf{M}_{ij} &= \sum^n \left([\mathbf{f}_i^k]_\times \mathbf{R}_{c_i c_j} \mathbf{f}_j^k \right) \left([\mathbf{f}_i^k]_\times \mathbf{R}_{c_i c_j} \mathbf{f}_j^k \right)^\top \end{aligned} \quad (10)$$

where $\lambda_{\mathbf{M}_{ij}, \min}$ represents the smallest eigenvalue of \mathbf{M}_{ij} .

Drawing inspiration from Kneip and Lynen's research [12], He et al. [13] utilize the NEC approach to optimize gyroscope bias directly. This involves integrating image

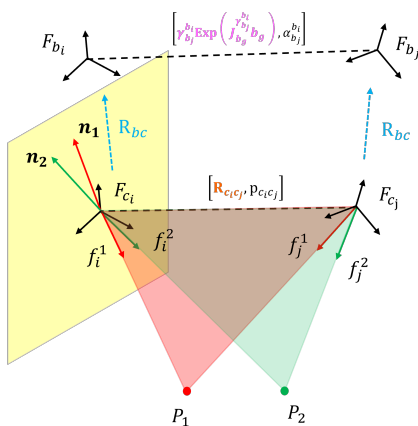


Fig. 1. Geometry of the normal epipolar constraint (NEC) and the relationship between gyroscope bias and NEC. The normal vectors \mathbf{n}_1 and \mathbf{n}_2 are perpendicular to the epipolar plane where $\mathbf{f}_i^1(\mathbf{f}_i^2)$ and $\mathbf{f}_j^1(\mathbf{f}_j^2)$ are located (red and green), and all normal vectors are in the same plane (yellow), forming a constraint that can be used to solve the rotation $\mathbf{R}_{c_i c_j}$ (orange). The problem of solving $\mathbf{R}_{c_i c_j}$ is transformed into the problem of solving the gyroscope bias (pink) by using the extrinsic parameter \mathbf{R}_{bc} (blue).

observations and the camera-IMU extrinsic calibration $\mathbf{T}_{bc} = [\mathbf{R}_{bc} | \mathbf{p}_{bc}]$.

$$\begin{aligned} \mathbf{R}_{c_i c_j} &= \mathbf{R}_{bc}^\top \mathbf{R}_{b_i b_j} \mathbf{R}_{bc} \\ \mathbf{p}_{c_i c_j} &= \mathbf{R}_{bc}^\top (\mathbf{p}_{b_i b_j} + \mathbf{R}_{b_i b_j} \mathbf{p}_{bc} - \mathbf{p}_{bc}) \end{aligned} \quad (11)$$

$\mathbf{R}_{b_i b_j}$ can be obtained by integrating the gyroscope measurements through Eq. (4). Substituting Eqs. (11) and (4) into Eq. (10), the objective function becomes:

$$\begin{aligned} \mathbf{b}_g^* &= \underset{\mathbf{b}_g}{\operatorname{argmin}} \lambda_{\mathbf{M}'_{ij}, \min} \\ \text{with } \mathbf{M}'_{ij} &= \sum_{k=1}^n \left([\mathbf{f}_i^k]_\times \mathbf{R}_{bc}^\top \gamma_{b_j}^{b_i} \operatorname{Exp} \left(\mathbf{J}_{\mathbf{b}_g}^{\gamma_{b_j}^{b_i}} \mathbf{b}_g \right) \mathbf{R}_{bc} \mathbf{f}_j^k \right)^\top \\ &\quad \left([\mathbf{f}_i^k]_\times \mathbf{R}_{bc}^\top \gamma_{b_j}^{b_i} \operatorname{Exp} \left(\mathbf{J}_{\mathbf{b}_g}^{\gamma_{b_j}^{b_i}} \mathbf{b}_g \right) \mathbf{R}_{bc} \mathbf{f}_j^k \right) \end{aligned} \quad (12)$$

which is one of the contributions in paper [13]. Fig. 1 illustrates the transformation in Eq. (12).

IV. PROPOSED APPROACH

Accurate estimation of the gyroscope bias plays a core role in improving the trajectory accuracy of VIO systems. The bias impacts the rotation, which in turn affects the integration of both translation and velocity. In this section, we present a method that can accurately solve the initialization parameters, which include gyroscope bias, velocity, gravity, and scale. The initialization process is divided into the following four steps: (1) gyroscope bias estimation, (2) rotation and translation estimation, (3) scale, velocity, and gravity estimation, and (4) scale and gravity refinement.

A. Gyroscope Bias Estimation

Considering that the image feature matches exhibit different error distributions, Muhle et al. [23] propose the probabilistic normal epipolar constraint (PNEC). Inspired by this, we aim to achieve a more accurate estimation of gyroscope bias by reducing the effect of uncertainty in the position of 2D feature points. To achieve this, we introduce the uncertainty of feature positions in the gyroscope bias optimizer. Assign an anisotropic covariance matrix to each feature point to represent this uncertainty. Given two consecutive image frames \mathbf{F}_{c_i} and \mathbf{F}_{c_j} , we first apply the method from PNEC to extract the 3D covariance matrix Σ_k for each unit bearing vector in \mathbf{F}_{c_j} . PNEC assumes that the position error in the image plane follows a 2D Gaussian distribution, with each feature characterized by a known 2D covariance matrix $\Sigma_{2D,k}$. Using Laplace's approximation, we can derive the 2D covariance matrix for KLT tracks from the KLT energy function. Given the 2D covariance matrix $\Sigma_{2D,k}$ of the feature position in \mathbf{F}_{c_j} , the unscented transform [24] is applied to propagate it through the unprojection function. This process yields the 3D covariance matrix Σ_k of the unit bearing vector \mathbf{f}_j^k in \mathbf{F}_{c_j} . Then based on the 3D covariance we can derive a probability distribution for the

NEC residuals, which is a univariate Gaussian distribution $\mathcal{N}(0, \sigma_k^2)$ with variance:

$$\sigma_k^2 = \mathbf{p}_{c_i c_j}^\top \left[\mathbf{f}_i^k \right]_\times \mathbf{R}_{c_i c_j} \Sigma_k \mathbf{R}_{c_i c_j}^\top \left[\mathbf{f}_i^k \right]_\times^\top \mathbf{p}_{c_i c_j} \quad (13)$$

To integrate this variance into an eigenvalue-based gyroscope bias estimation equation, we employ an optimization scheme analogous to the well-known iteratively reweighted least-square (IRLS) algorithm [25]. Based on Eq. (12), we define the weighted matrix incorporating the variance as:

$$\begin{aligned} \mathbf{M}_{ij}'' &= \sum_{k=1}^n \frac{\left(\left[\mathbf{f}_i^k \right]_\times \mathbf{R}_{c_i c_j} \mathbf{f}_j^k \right) \left(\left[\mathbf{f}_i^k \right]_\times \mathbf{R}_{c_i c_j} \mathbf{f}_j^k \right)^\top}{\tilde{\sigma}_k^2} \\ \mathbf{R}_{c_i c_j} &= \mathbf{R}_{bc}^\top \boldsymbol{\gamma}_{b_j}^{b_i} \text{Exp} \left(\mathbf{J}_{\mathbf{b}_g}^{\boldsymbol{\gamma}_{b_j}^{b_i}} \mathbf{b}_g \right) \mathbf{R}_{bc} \\ \tilde{\sigma}_k^2 &= \mathbf{p}_{pr}^\top \left[\mathbf{f}_i^k \right]_\times \mathbf{R}_{pr} \Sigma_k \mathbf{R}_{pr}^\top \left[\mathbf{f}_i^k \right]_\times^\top \mathbf{p}_{pr} \end{aligned} \quad (14)$$

where \mathbf{p}_{pr} and \mathbf{R}_{pr} denote the translation and rotation estimation of the previous frame. To take advantage of the IMU complementarity, we use the pre-integration results to compute the variance:

$$\begin{aligned} \tilde{\sigma}_k^2 &= \mathbf{p}_{pr}^\top \left[\mathbf{f}_i^k \right]_\times \mathbf{R}_{pr} \Sigma_k \mathbf{R}_{pr}^\top \left[\mathbf{f}_i^k \right]_\times^\top \mathbf{p}_{pr} \\ \mathbf{p}_{pr} &= \mathbf{R}_{bc}^\top (\boldsymbol{\alpha}_{pr} + \boldsymbol{\gamma}_{pr} \mathbf{p}_{bc} - \mathbf{p}_{bc}) \\ \mathbf{R}_{pr} &= \mathbf{R}_{bc}^\top \boldsymbol{\gamma}_{pr} \mathbf{R}_{bc} \end{aligned} \quad (15)$$

where $\boldsymbol{\alpha}_{pr}$ and $\boldsymbol{\gamma}_{pr}$ denote the translation and rotation pre-integration of the previous frame. Thus by incorporating variance, the eigenvalue-based gyroscope bias estimation problem is transformed into:

$$\begin{aligned} \mathbf{b}_g^* &= \underset{\mathbf{b}_g}{\text{argmin}} \lambda_{\mathbf{M}_{ij}'' \text{,min}} \\ \text{with } \mathbf{M}_{ij}'' &= \sum_{k=1}^n \frac{\left(\left[\mathbf{f}_i^k \right]_\times \mathbf{R}_{c_i c_j} \mathbf{f}_j^k \right) \left(\left[\mathbf{f}_i^k \right]_\times \mathbf{R}_{c_i c_j} \mathbf{f}_j^k \right)^\top}{\tilde{\sigma}_k^2} \\ \mathbf{R}_{c_i c_j} &= \mathbf{R}_{bc}^\top \boldsymbol{\gamma}_{b_j}^{b_i} \text{Exp} \left(\mathbf{J}_{\mathbf{b}_g}^{\boldsymbol{\gamma}_{b_j}^{b_i}} \mathbf{b}_g \right) \mathbf{R}_{bc} \end{aligned} \quad (16)$$

Given that the gyroscope bias varies slowly over time, it can be assumed to be constant during VIO initialization. Consequently, any keyframe pair $(i, j) \in \mathcal{E}$ that exhibits sufficient common features can be employed to estimate the gyroscope bias. \mathcal{E} denote the pairs of keyframes that satisfy the conditions during initialization that are used to optimize the solution:

$$\begin{aligned} \mathbf{b}_g^* &= \underset{\mathbf{b}_g}{\text{argmin}} \lambda \\ \text{with } \lambda &= \sum_{(i,j) \in \mathcal{E}} \lambda_{\mathbf{M}_{ij}'' \text{,min}} \end{aligned} \quad (17)$$

We use the Levenberg-Marquardt algorithm with the rotation parameterized based on the Cayley transformation [12] to solve Eq. (17). This allows us to initialize the gyroscope bias by minimizing the smallest eigenvalue λ . After solving for \mathbf{b}_g , we remove the gyroscope bias and reintegrate the gyroscope measurements. Finally, we can obtain accurate rotation estimations for both IMU frames and image frames.

B. Velocity, Gravity and Scale Estimation

After obtaining the rotation estimation, we start to solve for velocity, gravity, and scale. Additionally, we introduce a refinement module to further refine gravity and scale.

1) *LiGT for Position Estimation*: Before proceeding to the second part of the initialization, we need to solve for the translations between image frames. In this work, we set the first image frame as the world coordinate system. The position of each subsequent frame in this coordinate system is determined by applying a linear global translation constraint (LiGT) [14]. This constraint can handle collinear motions and local pure rotations, providing a more reliable translation estimation. LiGT requires three keyframes to construct the constraints, their indexes are defined as l, i, r . Then the LiGT can be expressed as:

$$\mathbf{B} \mathbf{p}_{c_0 c_r} + \mathbf{C} \mathbf{p}_{c_0 c_i} + \mathbf{D} \mathbf{p}_{c_0 c_l} = 0, \quad 0 \leq i \leq n, i \neq l \quad (18)$$

where

$$\begin{aligned} \mathbf{B} &= \left[\mathbf{f}_i^k \right]_\times \mathbf{R}_{c_i c_l} \mathbf{f}_l^k \mathbf{a}_{lr}^\top \mathbf{R}_{c_r c_0} \\ \mathbf{C} &= \theta_{lr}^2 \left[\mathbf{f}_i^k \right]_\times \mathbf{R}_{c_i c_0} \\ \mathbf{D} &= -(\mathbf{B} + \mathbf{C}) \\ \mathbf{a}_{lr}^\top &= \left(\left[\mathbf{R}_{c_r c_l} \mathbf{f}_l^k \right]_\times \mathbf{f}_r^k \right)^\top \left[\mathbf{f}_r^k \right]_\times \\ \theta_{lr} &= \left\| \left[\mathbf{f}_r^k \right]_\times \mathbf{R}_{c_r c_l} \mathbf{f}_l^k \right\| \end{aligned} \quad (19)$$

During initialization, a total of n ($n > 3$) keyframes are available, which allows for the construction of multiple LiGT constraints. By simultaneously solving multiple constraints, we can determine the translation $\mathbf{P} = [\mathbf{p}_{c_0 c_1}, \dots, \mathbf{p}_{c_0 c_n}]$ of all images in the world coordinate system relative to the initial frame. The rotation-translation-decoupled architecture helps us to overcome the visual SfM limitations and makes our approach more robust and efficient.

2) *Initializing Velocity, Gravity and Scale*: With the rotation and translation between images obtained, we can start initializing the following variables:

$$\mathcal{X} = [\mathbf{v}_{b_0}^{b_0}, \mathbf{v}_{b_1}^{b_1}, \dots, \mathbf{v}_{b_n}^{b_n}, s, \mathbf{g}^{c_0}] \quad (20)$$

where $\mathbf{v}_{b_n}^{b_n}$ denotes the IMU velocity at the moment n in \mathbf{F}_{b_n} , and s denotes the scale factor. For two consecutive IMU frames \mathbf{F}_{b_i} and \mathbf{F}_{b_k} , the following equation describes the relationship between metric position and velocity constraint with camera pose [10]:

$$\begin{aligned} \hat{\boldsymbol{\alpha}}_{b_k}^{b_i} &= \mathbf{R}_{b_i c_0} \left(s (\mathbf{p}_{c_0 b_k} - \mathbf{p}_{c_0 b_i}) + \frac{1}{2} \mathbf{g}^{c_0} \Delta t_{ik}^2 \right) - \mathbf{v}_{b_i}^{b_i} \Delta t_{ik} \\ \hat{\boldsymbol{\beta}}_{b_k}^{b_i} &= \mathbf{R}_{b_i c_0} \left(\mathbf{R}_{c_0 b_k} \mathbf{v}_{b_k}^{b_k} + \mathbf{g}^{c_0} \Delta t_{ik} \right) - \mathbf{v}_{b_i}^{b_i} \end{aligned} \quad (21)$$

Follow the equation $s \mathbf{p}_{c_0 b_k} = s \mathbf{p}_{c_0 c_k} - \mathbf{R}_{c_0 b_k} \mathbf{p}_{bc}$ in [13] and substitute it into Eq. (21):

$$\begin{aligned} \hat{\boldsymbol{\alpha}}_{b_k}^{b_i} &= s \mathbf{R}_{b_i c_0} (\mathbf{p}_{c_0 c_k} - \mathbf{p}_{c_0 c_i}) - \mathbf{R}_{b_i c_0} \mathbf{R}_{c_0 b_k} \mathbf{p}_{bc} \\ &\quad + \mathbf{p}_{bc} + \frac{1}{2} \mathbf{R}_{b_i c_0} \mathbf{g}^{c_0} \Delta t_{ik}^2 - \mathbf{v}_{b_i}^{b_i} \Delta t_{ik} \\ \hat{\boldsymbol{\beta}}_{b_k}^{b_i} &= \mathbf{R}_{b_i c_0} \mathbf{R}_{c_0 b_k} \mathbf{v}_{b_k}^{b_k} + \mathbf{R}_{b_i c_0} \mathbf{g}^{c_0} \Delta t_{ik} - \mathbf{v}_{b_i}^{b_i} \end{aligned} \quad (22)$$

To minimize the residuals between the predicted and measured values of translation and velocity, we create the following least-square problem:

$$\min_{\mathcal{X}} \sum_{(i,k) \in \mathcal{E}} \left\| \begin{bmatrix} \alpha_{b_k}^{b_i} - \hat{\alpha}_{b_k}^{b_i} \\ \beta_{b_k}^{b_i} - \hat{\beta}_{b_k}^{b_i} \end{bmatrix} \right\|^2, \quad (23)$$

Combining Eqs. (22) and (23), we obtain the following least-square solution:

$$\mathbf{H}' \begin{bmatrix} \mathbf{v}_{b_i}^{b_i} \\ \mathbf{v}_{b_k}^{b_k} \\ s \\ \mathbf{g}^{c_0} \end{bmatrix} = \mathbf{b}' \quad (24)$$

where

$$\mathbf{H}' = [\mathbf{A} \quad \mathbf{B}]$$

$$\begin{aligned} \mathbf{b}' &= \begin{bmatrix} \alpha_{b_k}^{b_i} - \mathbf{p}_{bc} + \mathbf{R}_{b_i c_0} \mathbf{R}_{c_0 b_k} \mathbf{p}_{bc} \\ \beta_{b_k}^{b_i} \end{bmatrix} \\ \mathbf{A} &= \begin{bmatrix} -\mathbf{I} \Delta t_{ik} & \mathbf{0} \\ -\mathbf{I} & \mathbf{R}_{b_i c_0} \mathbf{R}_{c_0 b_k} \end{bmatrix} \\ \mathbf{B} &= \begin{bmatrix} \mathbf{R}_{b_i c_0} (\mathbf{p}_{c_0 c_k} - \mathbf{p}_{c_0 c_i}) & \frac{1}{2} \mathbf{R}_{b_i c_0} \Delta t_{ik}^2 \\ \mathbf{0} & \mathbf{R}_{b_i c_0} \Delta t_{ik} \end{bmatrix} \end{aligned} \quad (25)$$

By solving the least-square problem, the velocity and the gravity as well as the scale can be obtained.

3) *Scale and Gravity Refinement*: Accurate estimation of gravity is required to improve the performance of VIO system. This is because gravity affects the observability and integration of translation and velocity. Additionally, a precise scale factor is needed to align the visual structure with the metric scale, which can enhance the system's accuracy. Therefore, we introduce gravity magnitude G [11] to refine both gravity and scale. Let $\mathbf{g}^I = \{0, 0, 1\}$ be the gravity direction of the inertial reference I. Based on the gravity \mathbf{g}^{c_0} obtained in the previous step, we can calculate the rotation $\mathbf{R}_{c_0 I}$:

$$\mathbf{R}_{c_0 I} = \text{Exp}(\mathbf{v}\theta)$$

$$\mathbf{v} = \frac{\mathbf{g}^I \times \mathbf{g}^{c_0}}{\|\mathbf{g}^I \times \mathbf{g}^{c_0}\|}, \quad \theta = \text{atan} 2(\|\mathbf{g}^I \times \mathbf{g}^{c_0}\|, \mathbf{g}^I \cdot \mathbf{g}^{c_0}) \quad (26)$$

the new gravity is then expressed as:

$$\hat{\mathbf{g}}^{c_0} = \mathbf{R}_{c_0 I} \mathbf{g}^I \quad (27)$$

The rotation matrix $\mathbf{R}_{c_0 I}$ can be parametrized with just two angles around the x and y axes in I, as a rotation around the z axis has no effect in \mathbf{g}^{c_0} [11]. By introducing a perturbation $\delta\theta$, we can optimize the rotation as follows:

$$\begin{aligned} \hat{\mathbf{g}}^{c_0} &= \mathbf{R}_{c_0 I} \text{Exp}(\delta\theta) \mathbf{g}^I \\ \delta\theta &= [\delta\theta_{xy}^\top \quad 0]^\top \\ \delta\theta_{xy} &= [\delta\theta_x \quad \delta\theta_y]^\top \end{aligned} \quad (28)$$

with a first-order approximation:

$$\hat{\mathbf{g}}^{c_0} \approx \mathbf{R}_{c_0 I} \mathbf{g}^I - \mathbf{R}_{c_0 I} [\mathbf{g}^I]_\times G \delta\theta \quad (29)$$

Substituting $s \mathbf{p}_{c_0 b_k} = s \mathbf{p}_{c_0 c_k} - \mathbf{R}_{c_0 b_k} \mathbf{p}_{bc}$ into Eq. (5), we have:

$$\begin{aligned} s \mathbf{p}_{c_0 c_j} &= s \mathbf{p}_{c_0 c_i} + \mathbf{v}_{b_i}^{c_0} \Delta t_{ij} - \frac{1}{2} \mathbf{g}^{c_0} \Delta t_{ij}^2 \\ &\quad + \mathbf{R}_{c_0 b_i} \alpha_{b_j}^{b_i} + (\mathbf{R}_{c_0 b_j} - \mathbf{R}_{c_0 b_i}) \mathbf{p}_{bc} \end{aligned} \quad (30)$$

Then according to Eqs. (29) and (30), we can derive:

$$\begin{aligned} s \mathbf{p}_{c_0 c_j} &= s \mathbf{p}_{c_0 c_i} + \mathbf{v}_{b_i}^{c_0} \Delta t_{ij} + \frac{1}{2} \mathbf{R}_{c_0 I} [\mathbf{g}^I]_\times G \Delta t_{ij}^2 \delta\theta \\ &\quad - \frac{1}{2} \mathbf{R}_{c_0 I} \mathbf{g}^I \Delta t_{ij}^2 + \mathbf{R}_{c_0 b_i} \alpha_{b_j}^{b_i} + (\mathbf{R}_{c_0 b_j} - \mathbf{R}_{c_0 b_i}) \mathbf{p}_{bc} \end{aligned} \quad (31)$$

We consider two connections between three consecutive keyframes i , j , and k . Using Eq. (6), we eliminate the velocity, resulting in the following equation:

$$[\lambda(i) \quad \phi(i)] \begin{bmatrix} s \\ \delta\theta_{xy} \end{bmatrix} = \psi(i) \quad (32)$$

where

$$\begin{aligned} \lambda(i) &= (\mathbf{p}_{c_0 c_j} - \mathbf{p}_{c_0 c_i}) \Delta t_{jk} - (\mathbf{p}_{c_0 c_k} - \mathbf{p}_{c_0 c_j}) \Delta t_{ij} \\ \phi(i) &= \frac{1}{2} \mathbf{R}_{c_0 I} [\mathbf{g}^I]_\times G (\Delta t_{ij}^2 \Delta t_{jk} + \Delta t_{jk}^2 \Delta t_{ij}) \\ \psi(i) &= (\mathbf{R}_{c_0 b_j} - \mathbf{R}_{c_0 b_i}) \mathbf{p}_{bc} \Delta t_{jk} - (\mathbf{R}_{c_0 b_k} - \mathbf{R}_{c_0 b_j}) \mathbf{p}_{bc} \Delta t_{ij} \\ &\quad + \mathbf{R}_{c_0 b_i} \alpha_{b_j}^{b_i} \Delta t_{ij} - \mathbf{R}_{c_0 b_i} \beta_{b_j}^{b_i} \Delta t_{ij} \Delta t_{jk} - \mathbf{R}_{c_0 b_j} \alpha_{b_k}^{b_j} \Delta t_{jk} \\ &\quad - \frac{1}{2} \mathbf{R}_{c_0 I} \mathbf{g}^I (\Delta t_{ij}^2 \Delta t_{jk} + \Delta t_{jk}^2 \Delta t_{ij}) \end{aligned} \quad (33)$$

In all the frames involved in initialization, each of the three consecutive keyframes forms an equation. Combining all the equations, we set up a system of linear equations. This system of equations can be effectively solved using Singular Value Decomposition (SVD) to determine the scale factor s and gravity direction correction $\delta\theta_{xy}$. Finally by updating $\mathbf{R}_{c_0 I}$ we complete the scale and gravity refinement.

V. EXPERIMENTS

In this section, we evaluate the proposed IMU initialization method in the EuRoC dataset [26]. The dataset includes synchronized global shutter WVGA stereo images at 20Hz, IMU measurements at 200Hz, and ground-truth trajectory information. The dataset comprises 11 sequences captured from a micro aerial vehicle (MAV). The sequences cover easy, medium, and difficult scenarios. We divided all the sequences collected into several data segments. Each data segment used for initialization consists of 10 keyframes obtained by sampling image frames at a frequency of 4Hz as used in [13]. We evaluate the performance of each algorithm using gyroscope bias error, velocity error, gravity direction error, and scale error. The Umeyama alignment [27] is employed to compute the scale error between the estimated trajectory and the ground truth trajectory. In experiments, we consider a scale error of less than one as a successful initialization and use the Root Mean Square Error (RMSE)

Dataset		MH01	MH02	MH03	MH04	MH05	V101	V102	V103	V201	V202	V203
Scale RMSE	VINS-Mono	0.147	0.165	0.166	0.169	0.195	0.143	0.150	0.252	0.196	0.174	0.281
	DRT-t	0.188	0.158	0.121	0.226	0.240	0.149	0.061	0.113	0.146	0.065	0.106
	DRT-I	0.097	0.112	0.085	0.167	0.164	0.113	0.078	0.178	0.106	0.085	0.156
	Ours	0.095	0.094	0.081	0.165	0.157	0.111	0.080	0.178	0.105	0.081	0.178
Velocity RMSE (m/s)	VINS-Mono	0.063	0.071	0.175	0.156	0.140	0.062	0.145	0.211	0.061	0.075	0.142
	DRT-t	0.088	0.080	0.125	0.197	0.182	0.069	0.072	0.128	0.062	0.056	0.095
	DRT-I	0.052	0.056	0.092	0.155	0.135	0.050	0.077	0.150	0.043	0.055	0.101
	Ours	0.051	0.051	0.087	0.154	0.133	0.048	0.076	0.140	0.044	0.054	0.102
G.Dir RMSE (°)	VINS-Mono	1.172	1.112	1.486	1.206	1.311	3.205	2.544	2.688	1.358	1.258	4.355
	DRT-t	0.959	0.949	0.931	1.087	0.992	3.155	0.850	1.657	1.064	0.856	1.278
	DRT-I	0.938	0.934	0.863	1.001	0.901	3.215	0.861	1.798	1.052	0.956	1.065
	Ours	0.652	0.621	0.606	0.704	0.630	2.752	0.727	1.399	0.808	1.014	1.091

TABLE I

DETAILED INITIALIZATION RESULTS FOR THE 10KFS SETTING IN EACH DATASET FROM EUROC. FOR EACH METRIC, THE BEST RESULT IS HIGHLIGHTED IN **RED**, THE SECOND BEST IN **BLUE**.

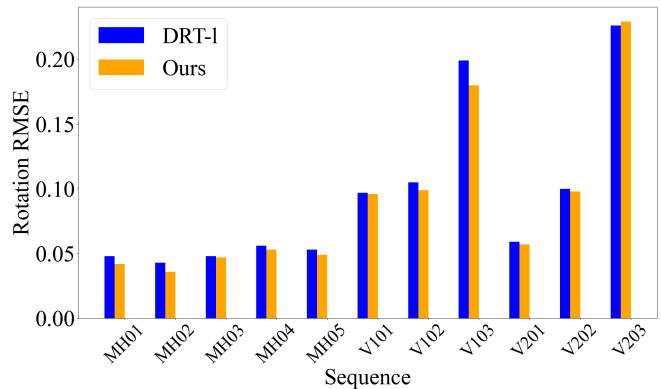
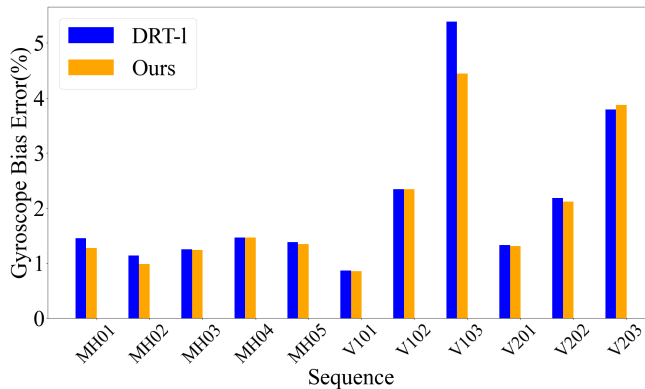


Fig. 2. Gyroscope bias errors and rotation RMSE on EuRoC sequences.

to evaluate the method. For comparison, we perform the same comprehensive test for the initialization methods DRT-t and DRT-I in [13], and for the loosely coupled initialization method in VINS-Mono (denoted as VINS-Mono) [16]. All algorithms undergo identical image processing operations. Existing features are tracked using the KLT sparse optical flow algorithm [28], while new corner features [29] are detected to maintain a consistent count of 150 points for each image. To mitigate outliers, we employ RANSAC with a fundamental matrix model [30]. All experiments are conducted on an Intel i7-9700 desktop with 32 GB of RAM.

A. Accuracy Evaluation

We compared the scale, gravity, and velocity estimated by the four methods on 1262 data segments in 11 sequences. From Table I, we can see that our method outperforms state-of-the-art initialization methods in almost all sequences, which verifies the effectiveness of our method. In terms of velocity and scale estimation, the tightly coupled method DRT-t is not as accurate as the loosely coupled DRT-I and ours. It is because DRT-t needs to integrate the IMU data from the initial moment to obtain velocity and position. This process is affected by noise, which degrades the accuracy

of scale and velocity. In terms of gravity estimation, our method greatly reduces the gravity error and validates the effectiveness of the scale-gravity refinement module. Comparing VINS-Mono and DRT-t, it can be seen that the rotation-translation-decoupled framework architecture has advantages in gravity estimation.

It should be noted that the main contribution of the LiGT constraint lies in its computational efficiency [13]. Therefore, the primary reason for the accuracy improvement is accurate rotation estimation. This observation indicates the importance of gyroscope bias estimation and the effectiveness of our method. We compare with DRT-I to verify the accuracy and robustness of our PNEC-based gyroscope bias estimation algorithm. Fig. 2 shows that in almost all sequences our method is more accurate than the previous best method DRT-I in gyroscope bias estimation. Owing to more precise gyroscope bias estimation, our method can obtain more accurate rotation through IMU pre-integration. Accurate rotation can improve trajectory accuracy and enhance the performance of the VIO system. The precise rotation estimation, combined with the advantage that the loosely coupled architecture is less affected by integration errors, makes our method outperform other methods in all three metrics.

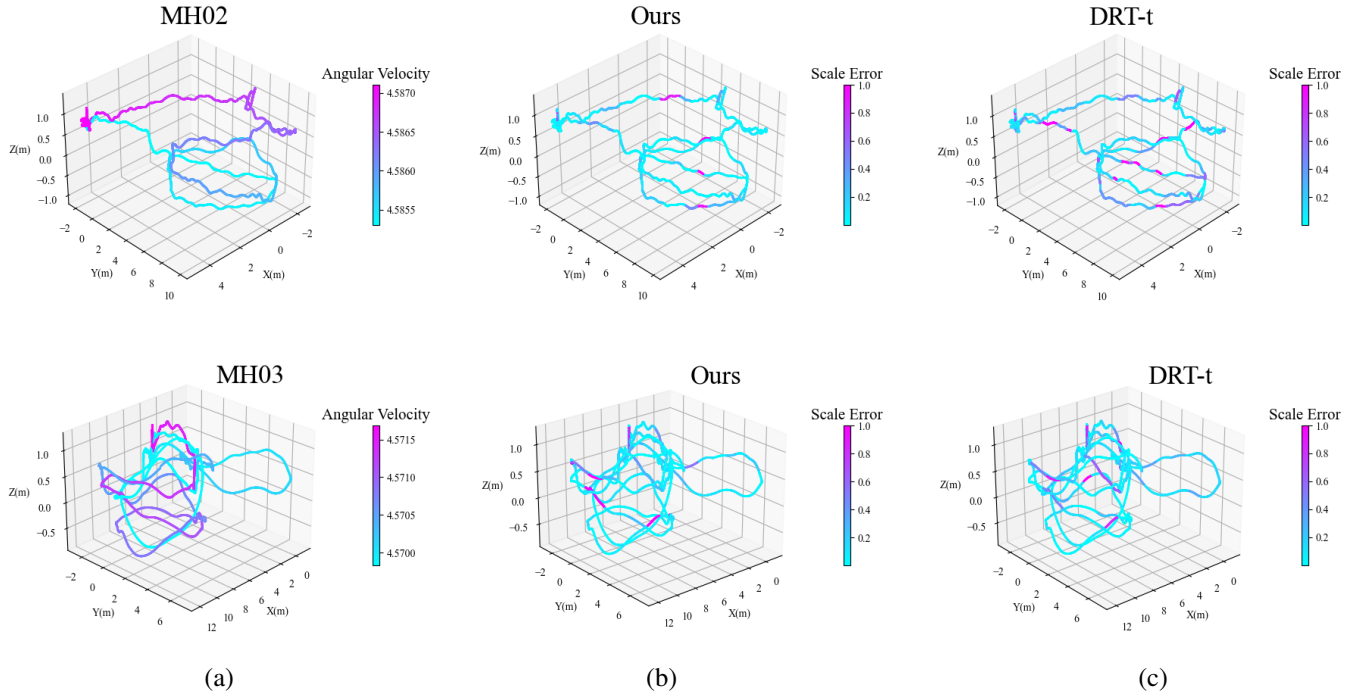


Fig. 3. Angular velocity and scale error visualizations for the MH02 dataset and MH03 dataset. The first-row image is MH02, and the second-row image is MH03. The column (a) shows the trajectory of the corresponding dataset colored based on the angular velocity. The columns (b) and (c) show the trajectory of our method and the DRT-t method based on the scale error colored on the corresponding dataset, respectively. The scale error is between 0 and 1. The lighter the color, the smaller the error.

Module	VINS-Mono	DRT-t	DRT-I	Ours
SfM	29.24	-	-	-
3D Cov Gen.	-	-	-	0.22
Bg Est.	0.93	3.63	3.68	3.62
Vel&Grav Est.	0.19	2.73	1.12	1.24
Sca&Grav Ref.	-	-	-	0.15
Total runtime	30.36	6.36	4.80	5.23

TABLE II

THE AVERAGE INITIALIZATION TIME IN MILLISECONDS ON THE EUROC DATASET. WE CALCULATE THE RUNTIME FOR SfM, 3D COVARIANCE GENERATION, GYROSCOPE BIAS ESTIMATION, VELOCITY AND GRAVITY ESTIMATION, AND SCALE-GRAVITY REFINEMENT.

B. Robustness Evaluation

To conduct robustness analysis, we visualize the trajectories of various datasets and color them based on the scale errors obtained from the solution. The scale error is a crucial metric for evaluating the initialization process. We color initialization sequences with scale errors less than one and consider initialization failures (i.e., purple) with scale errors greater than or equal to one. As shown in Fig. 2, our algorithm consistently maintains low-scale errors and a high initialization success rate across different motion modes. Notably, our algorithm achieves reliable initialization even when the device exhibits high angular velocity. Compared to the tightly coupled DRT-t method, our approach demonstrates superior robustness and accuracy in scale estimation.

C. Running Time Evaluation

To demonstrate the runtime details of our method compared to DRT-I, DRT-t, and the initialization method of VINS-Mono, we separately calculate and sum the runtime of each module for comparison. We run these four methods on 11 sequences of the EuRoC dataset and calculate the average runtime for each method in the gyroscope bias estimation and velocity-gravity estimation. Due to the need to compute the 3D covariance matrix and perform scale-gravity refinement, our method theoretically requires longer runtime. Table II shows the runtime of each module in the 10KFs setup for four initialization methods. We can see that the initialization speed of DRT-I is still the fastest. Due to additional modules, our method is on average 0.43 milliseconds slower than DRT-I, but 1.13 milliseconds faster than DRT-t. This is because DRT-t requires long-time integration of accelerometer data from the initial moment. In addition, our method is five times faster than the loosely coupled method VINS-Mono, since VINS-Mono uses SfM to compute camera trajectories and requires significantly longer runtime. In conclusion, our initialization method meets the real-time performance requirements of VIO systems.

VI. CONCLUSION

We propose a robust and accurate visual-inertial initialization method based on a rotation-translation-decoupled framework. A new gyroscope bias estimation formula is derived by establishing a probabilistic normal epipolar constraint, which directly utilizes visual observation and calculates

the uncertainty of feature point positions. Then, a least-square problem is established based on IMU and visual measurements to estimate velocity, scale, and gravity. Finally, an improved scale-gravity refinement module is introduced. Numerous initialization experiments have shown that our method improves accuracy and robustness while maintaining high computational efficiency. A limitation of the proposed method is that it does not consider the effect of accelerometer bias on velocity and scale. In the future, we will investigate a scale-gravity refinement module that covers accelerometer bias.

REFERENCES

- [1] W. Fang, L. Zheng, H. Deng, and H. Zhang, “Real-time motion tracking for mobile augmented/virtual reality using adaptive visual-inertial fusion,” *Sensors*, vol. 17, no. 5, p. 1037, 2017.
- [2] P. Li, T. Qin, B. Hu, F. Zhu, and S. Shen, “Monocular visual-inertial state estimation for mobile augmented reality,” in *2017 IEEE international symposium on mixed and augmented reality (ISMAR)*. IEEE, 2017, pp. 11–21.
- [3] J.-C. Piao and S.-D. Kim, “Adaptive monocular visual-inertial slam for real-time augmented reality applications in mobile devices,” *Sensors*, vol. 17, no. 11, p. 2567, 2017.
- [4] K. Sun, K. Mohta, B. Pfommer, M. Watterson, S. Liu, Y. Mulgaonkar, C. J. Taylor, and V. Kumar, “Robust stereo visual inertial odometry for fast autonomous flight,” *IEEE Robotics and Automation Letters*, vol. 3, no. 2, pp. 965–972, 2018.
- [5] Z. Yang, F. Gao, and S. Shen, “Real-time monocular dense mapping on aerial robots using visual-inertial fusion,” in *2017 IEEE International Conference on Robotics and Automation (ICRA)*. IEEE, 2017, pp. 4552–4559.
- [6] C. Campos, J. M. Montiel, and J. D. Tardós, “Inertial-only optimization for visual-inertial initialization,” in *2020 IEEE International Conference on Robotics and Automation (ICRA)*. IEEE, 2020, pp. 51–57.
- [7] A. Martinelli, “Closed-form solution of visual-inertial structure from motion,” *International journal of computer vision*, vol. 106, no. 2, pp. 138–152, 2014.
- [8] J. Kaiser, A. Martinelli, F. Fontana, and D. Scaramuzza, “Simultaneous state initialization and gyroscope bias calibration in visual inertial aided navigation,” *IEEE Robotics and Automation Letters*, vol. 2, no. 1, pp. 18–25, 2016.
- [9] J. Domínguez-Conti, J. Yin, Y. Alami, and J. Civera, “Visual-inertial slam initialization: A general linear formulation and a gravity-observing non-linear optimization,” in *2018 IEEE International Symposium on Mixed and Augmented Reality (ISMAR)*. IEEE, 2018, pp. 37–45.
- [10] T. Qin and S. Shen, “Robust initialization of monocular visual-inertial estimation on aerial robots,” in *2017 IEEE/RSJ International Conference on Intelligent Robots and Systems (IROS)*. IEEE, 2017, pp. 4225–4232.
- [11] R. Mur-Artal and J. D. Tardós, “Visual-inertial monocular slam with map reuse,” *IEEE Robotics and Automation Letters*, vol. 2, no. 2, pp. 796–803, 2017.
- [12] L. Kneip and S. Lynen, “Direct optimization of frame-to-frame rotation,” in *Proceedings of the IEEE International Conference on Computer Vision*, 2013, pp. 2352–2359.
- [13] Y. He, B. Xu, Z. Ouyang, and H. Li, “A rotation-translation-decoupled solution for robust and efficient visual-inertial initialization,” in *Proceedings of the IEEE/CVF Conference on Computer Vision and Pattern Recognition*, 2023, pp. 739–748.
- [14] Q. Cai, L. Zhang, Y. Wu, W. Yu, and D. Hu, “A pose-only solution to visual reconstruction and navigation,” *IEEE Transactions on Pattern Analysis and Machine Intelligence*, vol. 45, no. 1, pp. 73–86, 2021.
- [15] C. Campos, R. Elvira, J. J. G. Rodríguez, J. M. Montiel, and J. D. Tardós, “Orb-slam3: An accurate open-source library for visual, visual-inertial, and multimap slam,” *IEEE Transactions on Robotics*, vol. 37, no. 6, pp. 1874–1890, 2021.
- [16] T. Qin, P. Li, and S. Shen, “Vins-mono: A robust and versatile monocular visual-inertial state estimator,” *IEEE Transactions on Robotics*, vol. 34, no. 4, pp. 1004–1020, 2018.
- [17] P. Geneva, K. Eckenhoff, W. Lee, Y. Yang, and G. Huang, “Openvins: A research platform for visual-inertial estimation,” in *2020 IEEE International Conference on Robotics and Automation (ICRA)*. IEEE, 2020, pp. 4666–4672.
- [18] J. Engel, V. Koltun, and D. Cremers, “Direct sparse odometry,” *IEEE transactions on pattern analysis and machine intelligence*, vol. 40, no. 3, pp. 611–625, 2017.
- [19] R. Mur-Artal and J. D. Tardós, “Orb-slam2: An open-source slam system for monocular, stereo, and rgbd cameras,” *IEEE transactions on robotics*, vol. 33, no. 5, pp. 1255–1262, 2017.
- [20] D. Zuniga-Noël, F.-A. Moreno, and J. Gonzalez-Jimenez, “An analytical solution to the imu initialization problem for visual-inertial systems,” *IEEE Robotics and Automation Letters*, vol. 6, no. 3, pp. 6116–6122, 2021.
- [21] C. Forster, L. Carbone, F. Dellaert, and D. Scaramuzza, “On-manifold preintegration for real-time visual-inertial odometry,” *IEEE Transactions on Robotics*, vol. 33, no. 1, pp. 1–21, 2016.
- [22] L. Kneip, R. Siegwart, and M. Pollefeys, “Finding the exact rotation between two images independently of the translation,” in *Computer Vision-ECCV 2012: 12th European Conference on Computer Vision, Florence, Italy, October 7–13, 2012, Proceedings, Part VI* 12. Springer, 2012, pp. 696–709.
- [23] D. Muhle, L. Koestler, N. Demmel, F. Bernard, and D. Cremers, “The probabilistic normal epipolar constraint for frame-to-frame rotation optimization under uncertain feature positions,” in *Proceedings of the IEEE/CVF Conference on Computer Vision and Pattern Recognition*, 2022, pp. 1819–1828.
- [24] J. K. Uhlmann, “Dynamic map building and localization: New theoretical foundations,” Ph.D. dissertation, University of Oxford Oxford, 1995.
- [25] C. L. Lawson, “Contribution to the theory of linear least maximum approximation,” *Ph. D. dissertation. Univ. Calif.*, 1961.
- [26] M. Burri, J. Nikolic, P. Gohl, T. Schneider, J. Rehder, S. Omari, M. W. Achtelik, and R. Siegwart, “The euroc micro aerial vehicle datasets,” *The International Journal of Robotics Research*, vol. 35, no. 10, pp. 1157–1163, 2016.
- [27] S. Umeyama, “Least-squares estimation of transformation parameters between two point patterns,” *IEEE Transactions on Pattern Analysis & Machine Intelligence*, vol. 13, no. 04, pp. 376–380, 1991.
- [28] B. D. Lucas and T. Kanade, “An iterative image registration technique with an application to stereo vision,” in *IJCAI'81: 7th international joint conference on Artificial intelligence*, vol. 2, 1981, pp. 674–679.
- [29] J. Shi *et al.*, “Good features to track,” in *1994 Proceedings of IEEE conference on computer vision and pattern recognition*. IEEE, 1994, pp. 593–600.
- [30] R. Hartley and A. Zisserman, *Multiple view geometry in computer vision*. Cambridge university press, 2003.